

Robot Manipulation Task Learning by Leveraging $SE(3)$ Group Invariance and Equivariance

JooHwan Seo¹, Nikhil P. S. Prakash¹, Xiang Zhang¹, Changhao Wang¹,
Jongun Choi^{1,2}, Masayoshi Tomizuka¹, and Roberto Horowitz¹

Abstract—This paper presents a differential geometric control approach that leverages $SE(3)$ group invariance and equivariance to increase transferability in learning robot manipulation tasks that involve interaction with the environment. Specifically, we employ a control law and a learning representation framework that remain invariant under arbitrary $SE(3)$ transformations of the manipulation task definition. Furthermore, the control law and learning representation framework are shown to be $SE(3)$ equivariant when represented relative to the spatial frame. The proposed approach is based on utilizing a recently presented geometric impedance control (GIC) combined with a learning variable impedance control framework, where the gain scheduling policy is trained in a supervised learning fashion from expert demonstrations. A geometrically consistent error vector (GCEV) is fed to a neural network to achieve a gain scheduling policy that remains invariant to arbitrary translation and rotations. A comparison of our proposed control and learning framework with a well-known Cartesian space learning impedance control, equipped with a Cartesian error vector-based gain scheduling policy, confirms the significantly superior learning transferability of our proposed approach. A hardware implementation on a peg-in-hole task is conducted to validate the learning transferability and feasibility of the proposed approach.

I. INTRODUCTION

Learning has become a prevalent method for robots to acquire skills in automated manipulation tasks [1]. Most learning-based approaches are formulated using a Cartesian frame to represent the end-effector workspace. However, Cartesian-based learning formulations lack learning transferability in that trained policies cannot be directly transferred to arbitrarily translated/rotated task descriptions unless extensive additional training is conducted [2], [3].

From the differential geometric perspective, the poor transferability of trained policies can be directly attributed to the absence of $SE(3)$ group equivariance in the Cartesian-based learning framework. For instance, a group transformation (e.g. translation/rotation) of the task definition does not result in a corresponding transformation of trained policy and task execution. As a consequence, group-transformed tasks have

to be relearned, requiring a significant increase in training episodes and learning resources.

Recently, in the field of geometric deep learning (GDL) in computer vision applications [4], [5], the symmetry inherent to a group structure within a domain has been exploited and integrated into neural network models to enhance learning transferability and robustness to untrained data, thereby improving sample efficiency. The key properties exploited by GDL are group invariance and equivariance. Invariance refers to a property of a map whose output remains unchanged when a group action transforms its input, while equivariance implies that a map's output is transformed by the representation of the same group action when its input is transformed by the group action.

Robotic manipulator workspaces have a group structure, which is frequently represented by the Special Euclidean group $SE(3)$ [6]. In our previous work [7], we introduced a geometric impedance control (GIC) for robot manipulators that fully incorporates the geometric structure of $SE(3)$. GIC leverages the left-invariance of the distance metric and potential function in $SE(3)$ to design a control law expressed in the body-frame coordinate system.

In this paper, we leverage $SE(3)$ group invariance and equivariance, extensively studied in GDL, to enhance learning transferability in contact-rich robotic manipulation tasks. A Peg-in-Hole (PiH) task is used as a testbed for evaluation, since it is sensitive to $SE(3)$ transformations (i.e. translation/rotation) and involves contact-rich robot interaction with the environment. A geometric learning variable impedance control is presented that utilizes the GIC in [7] and incorporates a learning variable impedance control framework, where the gain scheduling policy is trained in a supervised learning fashion from expert demonstrations. A geometrically consistent error vector (GCEV) is fed to a neural network to achieve a gain scheduling policy that remains invariant under arbitrary $SE(3)$ transformations. The main contributions of our paper are:

- 1) We propose a method of combining a geometric impedance control (GIC) and learning impedance gains to solve contact-rich robotic manipulation tasks, e.g., Peg-in-Hole. Under the proposed method, the learned policy can be transferred to other unexperienced positions/orientations of the target pose.
- 2) We prove that the GIC and the geometrically consistent error vector (GCEV) used for learning, when represented in the end-effector's body frame system, are

Research partially funded by (1) the Tsinghua-Berkeley Shenzhen Institute (TBSI) phase II and (2) the Hong Kong Center for Construction Robotics Limited (HKCRC). Jongun Choi was supported by the National Research Foundation of Korea (NRF) grant funded by the Korea government (MSIT). (No.RS-2023-00221762 and No.2021R1A2B5B01002620)

¹ UC Berkeley, Department of Mechanical Engineering. Emails: {jooHwan_seo, nikhilps, xiang.zhang_98, changhaowang, tomizuka, horowitz}@berkeley.edu

² Yonsei University, School of Mechanical Engineering. Email: joungeunchoi@yonsei.ac.kr

left-invariant relative to $SE(3)$ group transformations. This key property enables learning transferability using force-based policies.

- 3) We also show that the aforementioned left-invariance property leads to equivariance when the GIC and GCEV are both described relative to a spatial frame.
- 4) We validate the feasibility and transferability of our proposed robot manipulation task learning approach through an actual hardware implementation.

II. RELATED WORKS

A. Geometric Deep Learning for Robotics Problem

While GDL has achieved success in image-domain data, especially in medical fields [5], there have also been studies utilizing geometric approaches in robotics [8], [9], [10], [11]. The main intuition behind these geometric approaches is to exploit the invariance and equivariance of the group structure.

In [8], $SE(2)$ equivariance is exploited to achieve highly sample-efficient end-to-end learning for robotic manipulation tasks based on image inputs. On the other hand, $SE(3)$ equivariance is realized in [9], [10], [11] to deal with the point cloud input data. Tensor field network [11] was introduced to deal with point cloud input, providing spatial roto-translational ($SE(3)$) and permutation equivariance structure. In [9], a descriptor field with $SE(3)$ equivariance structure is utilized, greatly improving the performance for the out-of-distribution (OOD) inputs, and further advancements were made in [10]. However, to date, the use of GDL in robotic applications has only dealt with point cloud or image inputs and has not leveraged the kinematics and dynamics of the manipulator. In addition, they have rarely been combined with a dynamic controller, which raises a need for integrating GDL with dynamic controllers.

B. Peg-in-Hole task and Learning Variable Impedance Control

The Peg-in-Hole (PiH) task is a benchmark problem for force-controlled robotic manipulation tasks [12]. A widely utilized approach to solve a PiH task is the variable impedance control [3], [13], [2], where the controller's impedance gains change depending on the states. These approaches, however, do not take into account the geometric structures of the manipulator. As a result, it is reported in [2] that the success rate of a trained policy dropped significantly under $SE(3)$ transformation, i.e., when the peg position is tilted related to the orientation used for training. To deal with this issue, a typical approach is to adopt the domain randomization technique as in [3], where both the initial and goal poses of the end-effector are randomized during the training. In contrast, our proposed approach achieves robustness to OOD goal poses and learning transferability without randomizing goal poses during the training stage. We note that the proposed approach is not constrained to the PiH task, but it can be extended to other manipulation tasks with force interaction, such as surface wiping or pick-and-place.

III. GEOMETRIC IMPEDANCE CONTROL

A. Lie Groups and Manipulator Dynamics

The configuration of the manipulator's end-effector can be defined by its position and orientation, and the configuration manifold lies in the Special Euclidean group $SE(3)$. We can represent the end-effector's configuration frame $\{b\}$ using the following homogeneous matrix g_{sb} , to fixed (inertial) spatial frame $\{s\}$, as follows:

$$g_{sb} = \begin{bmatrix} R & p \\ 0 & 1 \end{bmatrix} \in SE(3). \quad (1)$$

Here, R is a rotation matrix and $R \in SO(3)$, a Special Orthogonal Group, which is defined as $SO(3) = \{R \in \mathbb{R}^{3 \times 3} | R^T R = R R^T = I, \det(R) = 1\}$, and $p \in \mathbb{R}^3$. We will drop the subscript s since the spatial coordinate frame can be considered an identity without loss of generality. In addition, we also drop the subscript b for the current configuration of the end-effector for the compactness of notation unless specified, i.e., $g_{sb} = g$. We also use $g = (R, p)$ for compactness of notation.

The Lie algebra of $SO(3)$, denoted by $so(3)$, defines skew-symmetric matrices. The *hat-map* for $so(3)$ is defined by $\widehat{(\cdot)} : \mathbb{R}^3 \rightarrow so(3)$, which maps a vector $\omega \in \mathbb{R}^3$ to its skew-symmetric matrix i.e., $\widehat{\omega} = -\widehat{\omega}^T$ for $\omega \in \mathbb{R}^3$. The inverse of the *hat-map*, $\widehat{(\cdot)}$, is the *vee-map* $(\cdot)^\vee : so(3) \rightarrow \mathbb{R}^3$. Similarly to $SO(3)$, the Lie algebra of $SE(3)$ is denoted by $se(3)$. The *hat-map* for $se(3)$ is defined as $\widehat{(\cdot)} : \mathbb{R}^6 \rightarrow se(3)$. The inverse map of *hat-map* is defined by *vee-map* $(\cdot)^\vee : se(3) \rightarrow \mathbb{R}^6$. The $se(3)$ representation can be summarized by

$$\widehat{\xi} = \begin{bmatrix} \widehat{\omega} & v \\ 0 & 0 \end{bmatrix} \in se(3), \quad \forall \xi = \begin{bmatrix} v \\ \omega \end{bmatrix} \in \mathbb{R}^6, \quad v, \omega \in \mathbb{R}^3, \quad \widehat{\omega} \in so(3).$$

For the details of the Lie group for robotic manipulators, we refer to [6], [14].

The forward kinematics of a manipulator with revolute joints can be described using Lie Group and matrix exponentials [6], i.e.,

$$g(q) = e^{\widehat{\xi}_1 q_1} \dots e^{\widehat{\xi}_n q_n} g(0) = \begin{bmatrix} R(q) & p(q) \\ 0 & 1 \end{bmatrix} \in SE(3), \quad (2)$$

where $q = [q_1, \dots, q_n]^T \in S^n$ is a joint coordinate for revolute joints, n is a number of joints, and $g(0)$ is an initial (zero) configuration.

The velocity of the end-effector relative to its body frame, $V^b \in \mathbb{R}^6$, can be calculated using the following formula:

$$V^b = \begin{bmatrix} v^b \\ \omega^b \end{bmatrix} = (g^{-1} \dot{g})^\vee, \quad (3)$$

i.e., $\dot{g} = g \widehat{V}^b$. The velocity V^b can also be computed using the body Jacobian matrix $J_b(q)$ via $V^b = J_b(q) \dot{q}$. For the details about $J_b(q)$, we refer to Chap 5.1 of [14].

The dynamic equations of motion for rigid-link robotic manipulators are given by:

$$M(q) \ddot{q} + C(q, \dot{q}) \dot{q} + G(q) = T + T_e, \quad (4)$$

where $M(q) \in \mathbb{R}^{n \times n}$ is the symmetric positive definite inertia matrix, $C(q, \dot{q}) \in \mathbb{R}^{n \times n}$ is a Coriolis matrix, $G(q) \in \mathbb{R}^n$ is a moment term due to gravity, $T \in \mathbb{R}^n$ is a control input, and $T_e \in \mathbb{R}^n$ is an external disturbance. As in [7], the manipulator

dynamics in operational space formulation [15], using the body-frame velocity, is represented as follows:

$$\tilde{M}(q)\dot{V}^b + \tilde{C}(q, \dot{q})V^b + \tilde{G}(q) = \tilde{T} + \tilde{T}_e, \text{ where} \quad (5)$$

$$\tilde{M}(q) = J_b(q)^{-T} M(q) J_b(q)^{-1},$$

$$\tilde{C}(q, \dot{q}) = J_b(q)^{-T} (C(q, \dot{q}) - M(q) J_b(q)^{-1} \dot{J}) J_b(q)^{-1},$$

$$\tilde{G}(q) = J_b(q)^{-T} G(q), \quad \tilde{T} = J_b(q)^{-T} T, \quad \tilde{T}_e = J_b(q)^{-T} T_e,$$

where $A^{-T} = (A^{-1})^T$. We will denote $\tilde{M}(q)$ as \tilde{M} , $\tilde{C}(q, \dot{q})$ as \tilde{C} and $\tilde{G}(q)$ as \tilde{G} for the rest of the paper.

B. Geometric Impedance Control Law

We employ the geometric impedance control (GIC) law proposed in [7]. We first note that g denotes the current configuration matrix, with p and R in (1) representing the current position and rotation matrix, i.e., $g = (R, p)$. In a similar way, $g_d = (R_d, p_d)$ denotes the desired current configuration matrix. In a nutshell, a GIC control law $\tilde{T} \in se^*(3)$ in the wrench is given by

$$\tilde{T} = \tilde{M}\dot{V}_{*d}^b + \tilde{C}V_{*d}^b + \tilde{G} - f_G - K_d e_V. \quad (6)$$

where \tilde{C} , and \tilde{G} are matrices in the operational space formulation (5), K_d is symmetric positive definite damping matrix, f_G is the elastic generalized force in $se^*(3)$ and e_V is a velocity error vector, both of them described on the body-frame, which will be described subsequently. The elastic geometric wrench (force) $f_G(g, g_d)$ is given by

$$f_G(g, g_d) = \begin{bmatrix} f_p \\ f_R \end{bmatrix} = \begin{bmatrix} R^T R_d K_p R_d^T (p - p_d) \\ (K_R R_d^T R - R^T R_d K_R)^\vee \end{bmatrix}, \quad (7)$$

where K_p and K_R denote symmetric positive definite stiffness matrices in translation and rotation, respectively. The current and desired velocity vectors cannot be directly compared, as they lie on different tangent spaces. Therefore, we utilize a vector translation map (Adjoint map) to first translate the desired velocity to the tangent space of the current velocity [16]. The error vector e_V is defined by

$$e_V = V^b - V_{*d}^b = \begin{bmatrix} e_v \\ e_\omega \end{bmatrix} \quad (8)$$

$$V_{*d}^b = \text{Ad}_{g_{bd}} V_d^b, \text{ with } \text{Ad}_{g_{bd}} = \begin{bmatrix} R_{bd} & \hat{p}_{bd} R_{bd} \\ 0 & R_{bd} \end{bmatrix},$$

where V_d^b is a desired velocity in the desired body frame, $\text{Ad}_{g_{bd}} : \mathbb{R}^6 \rightarrow \mathbb{R}^6$ is an Adjoint map, $R_{bd} = R^T R_d$, $p_{bd} = -R^T (p - p_d)$, and V_{*d}^b is a translated desired velocity on the configuration body-frame.

For the PiH task, we assumed that the final desired configuration g_d is given and is time-invariant, i.e., $\dot{g}_d(t) = 0$. Thus, the controller law (6) is modified as

$$\tilde{T} = -f_G - K_d V^b + \tilde{G}, \quad (9)$$

which can be interpreted as a PD control together with gravity compensation. For more details on the GIC, such as derivation and stability properties, we refer to [7] and its references [17], [16].

C. Distance Metric and Geometrically Consistent Error Vectors in $SE(3)$

We introduce a geometrically consistent error vector (GCEV) in $SE(3)$ which could be employed in learning manipulation tasks. A GCEV can be derived from the distance

metric. The distance metric proposed in [7] is given by

$$\Psi(g, g_d) = \frac{1}{2} \|I - g_d^{-1} g\|_F^2 = \text{tr}(I - R_d^T R) + \frac{1}{2} (p - p_d)^T (p - p_d), \quad (10)$$

where $\|\cdot\|_F$ denotes a Frobenius norm of a matrix. The GCEV $e_G(g, g_d)$ is then defined as follows:

$$e_G(g, g_d) = \begin{bmatrix} e_p \\ e_R \end{bmatrix} = \begin{bmatrix} R^T (p - p_d) \\ (R_d^T R - R^T R_d)^\vee \end{bmatrix} \in \mathbb{R}^6, \quad (11)$$

We introduce the following lemma to show that $e_G(g, g_d)$ and $f_G(g, g_d)$ are invariant to an arbitrary left transformation $g_l \in SE(3)$.

Lemma 1: Left-invariance of the GCEV (11) and the elastic wrench (7)

$e_G(g, g_d)$ and $f_G(g, g_d)$ are left-invariant to the arbitrary left-transformation $g_l \in SE(3)$.

Proof: Let $g_l = (R_l, p_l)$. Then, the left-transformed homogeneous matrix $g_l g$ is calculated in the following way:

$$g_l g = \begin{bmatrix} R_l & p_l \\ 0 & 1 \end{bmatrix} \begin{bmatrix} R & p \\ 0 & 1 \end{bmatrix} = \begin{bmatrix} R_l R & R_l p + p_l \\ 0 & 1 \end{bmatrix}$$

Similarly, $g_l g_d = (R_l R_d, R_l p_d + p_l)$. The left-transformed GCEV is then

$$e_G(g_l g, g_l g_d) = \begin{bmatrix} R^T R_l^T (R_l p + p_l - R_l p_d - p_l) \\ ((R_l R_d)^T R_l R - (R_l R)^T R_l R_d)^\vee \end{bmatrix} \quad (12)$$

$$= \begin{bmatrix} R^T (p - p_d) \\ (R_d^T R - R^T R_d)^\vee \end{bmatrix} = e_G(g, g_d)$$

Similarly, the left-transformed elastic wrench is

$$f_G(g_l g, g_l g_d) = \begin{bmatrix} (R_l R)^T R_l R_d K_p (R_l R_d)^T (R_l p + p_l - R_l p_d - p_l) \\ (K_R (R_l R_d)^T R_l R - (R_l R)^T R_l R_d K_R)^\vee \end{bmatrix}$$

$$= \begin{bmatrix} R^T R_d K_p R_d (p - p_d) \\ (K_R R_d R - R^T R_d K_R)^\vee \end{bmatrix} = f_G(g, g_d) \quad (13)$$

which shows the left-invariance of $e_G(g, g_d)$ and $f_G(g, g_d)$. ■

Finally, we note that all the vectors/wrench, such as e_G , e_V , and f_G , are described in the body-frame coordinate unless specified.

D. Cartesian space Impedance Control

As a benchmark approach for the proposed GIC, we also briefly introduce a Cartesian space Impedance Controller (CIC), which is widely utilized in the variable impedance control setup. In the operational space formulation, correctly representing the rotational dynamics has always received significant interest [18]. In particular, a positional Cartesian error vector e_C widely utilized in CIC can be defined in the following way [19], [20], [21].

$$e_C = [(e_{C,p})^T, (e_{C,R})^T]^T, \text{ where} \quad (14)$$

$$e_{C,p} = p - p_d, \quad e_{C,R} = (r_{d1} \times r_1 + r_{d2} \times r_2 + r_{d3} \times r_3),$$

with $R = [r_1, r_2, r_3]$ and $R_d = [r_{d1}, r_{d2}, r_{d3}]$. Utilizing the positional error vector in Cartesian space and considering a fair comparison with the GIC formulation, we will utilize the following CIC formulation for the PiH task.

$$\tilde{T}_C = -K_C e_C - K_{dC} V^s + \tilde{G}_C, \quad (15)$$

where \tilde{G}_C can be obtained by replacing J_b by J_s in (5), K_{dC} is a damping matrix for the CIC, and $K_C =$

$\text{blkdiag}(K_{C,p}, K_{C,r})$ with $K_{C,p}$ and $K_{C,r}$ are translational and rotational stiffness matrices, respectively. In addition, J_s denotes a spatial frame Jacobian matrix and $V^s = J_s \dot{q}$. To implement control law (9) and (15), the wrenches should first be converted to joint torque T in (4) by multiplying corresponding Jacobian matrices, i.e., $T = J_b^T \tilde{T}$ and $T = J_s^T \hat{T}_C$, respectively.

IV. LEARNING IMPEDANCE GAINS

A. Problem Setup

1) *Overview*: In the variable impedance control framework, we train a gain-scheduling policy using two different approaches: naive behavior cloning (BC) and reinforcement learning (RL). We assume that the exact hole position g_d is known. The inputs to the policy are positional error vectors of the GIC or the CIC, respectively denoted as e_G and e_C , while the outputs are the impedance gain matrices. Four scenarios are considered (Fig. 1), with the default scenario (Fig. 1(a)) used for training the policy. The trained policy is then tested in the other scenarios (Fig. 1s(b)-(d)) to evaluate its zero-shot transferability. All simulations are conducted in the Mujoco simulation environment [22] for environment setup and the Berkeley RL kit [23] for the RL training. The GitHub repository of this project is published in https://github.com/Joohwan-Seo/GIC_Learning_public.

2) *Action mapping*: To map the actions from BC and RL to impedance gains, we first consider diagonal components of the matrix gains K_p and K_R as follows:

$$K_p = \text{diag}([k_{p_1}, k_{p_2}, k_{p_3}]), \quad K_R = \text{diag}([k_{r_1}, k_{r_2}, k_{r_3}]).$$

The damping matrix K_d is fixed as

$$K_d = 8 \cdot \text{diag}([k_{p_1}, k_{p_2}, k_{p_3}, k_{r_1}, k_{r_2}, k_{r_3}])^{0.5} \quad (16)$$

For the task shown in Fig. 1(a), a symmetric structure is considered in the action mapping. Specifically, we have the same action mapping in the x and y directions (k_{p_1} and k_{p_2}) and a different mapping in the z direction. In the rotational part, the action mapping for k_{r_1} , k_{r_2} , and k_{r_3} is the same. The selected action mapping is as follows:

$$k_{p_i} = 10^{a_i+2.5}, \quad \text{for } i = 1, 2, \quad k_{p_3} = 10^{1.5 \cdot a_3+2.0},$$

$$k_{r_j} = 10^{0.6 \cdot a_j+2.0}, \quad \text{for } j = 1, 2, 3,$$

where a denotes an action, $a = [a_1, a_2, \dots, a_6]^T \in [-1, 1] \times \dots \times [-1, 1] \subset \mathbb{R}^6$.

3) *Domain Randomization*: Domain randomization is a crucial technique in both BC and RL to enhance robustness by allowing the neural network to explore a broader range of state space [24]. In traditional learning of impedance gains [3], domain randomization is typically applied to both the initial and goal end-effector poses. However, under the GIC framework, domain randomization is only necessary for the initial pose of the end-effector, as demonstrated in the following proposition.

Proposition 1: For the learning variable impedance control problem based on GIC law (6), randomization on the initial condition of the end-effector is all you need.

Proof: Since the main driving force of (6) for the given task is $f_G(g, g_d)$ (7), we focus on the properties of $f_G(g, g_d)$. According to lemma 1, $f_G(g, g_d)$ is left-invariant

to arbitrary $SE(3)$ transformation g_l acting on the left, i.e., $f_G(g_l g, g_l g_d) = f_G(g, g_d)$. Noting that arbitrarily located/tilted goal end-effector pose can be described by $g_l g_d$, the following equation holds:

$$f_G(g, g_l g_d) = f_G(g_l g_l^{-1} g, g_l g_d) = f_G(g_l^{-1} g, g_d). \quad (17)$$

Following the axioms of groups (Chap 2.1, [6]), g_l^{-1} is nothing but a group element in $SE(3)$ since it is arbitrary. ■

The conclusion of Proposition 1 states that when using GIC with a left-invariant gain scheduling policy, domain randomization on the end-effector's goal pose is not necessary, and thereby learning transferability is achieved. Therefore, we randomize the initial configuration $g_0 = (R_0, p_0)$ at the beginning of each episode.

4) *Scripted Expert Policy*: To collect the required dataset in the simulation environment, we developed a heuristic rule-based scripted expert policy. This expert policy is also utilized to facilitate exploration during the RL environment. The main intuition is to use small z gains and high gains in the x and y directions when the robot approaches the hole while using high z gains during the insertion to overcome the friction between the peg and the hole. As a result, the robot first aligns the peg with the hole's axis and then gradually pushes the peg into the hole. During data collection in BC and expert trajectory injection in RL, small amounts of noise are added to the scripted expert policy to enhance robustness.

B. Behavior Cloning (BC)

For the naive behavior cloning approach, we utilize a simple multi-layer perceptron (MLP)-based neural network as a policy parametrization. Formally, a neural network-based policy can be represented as $a_i = \mu_\theta(s_i)$, where $\mu_\theta(\cdot)$ is a neural network with learnable parameters θ , and s_i is an input state to the neural network. For GIC, $s_i = e_G \in \mathbb{R}^6$, and for CIC, $s_i = e_C \in \mathbb{R}^6$. We utilize a neural network with 3 layers, with the number of nodes per layer being 128. ReLU is employed for the hidden activation functions, and tanh is used for the output activation function to enforce the output range to be $[-1, 1]$. The learning problem for behavior cloning can be defined as $\theta^* = \arg \min_\theta \frac{1}{N} \sum_{i=1}^N \|a_i - \mu_\theta(s_i)\|_2^2$, where N is the length of the dataset, and $N = 10^6$ was used. The BC policy is trained following the standard deep learning fashion - stochastic gradient descent on a sampled batch dataset with an Adams optimizer, learning rate schedule, and early stopping.

C. Reinforcement Learning (RL)

In order to further demonstrate our concept, we applied reinforcement learning (RL) and utilized the Soft Actor-Critic (SAC) algorithm [25]. SAC is chosen because it is known to explore more and less likely to fall into the local optimum compared to other deep RL algorithms [26].

Solving the PiH task using RL is challenging because it is an exploration-sensitive problem. Previous works [12], [3], [27] tackling the PiH task with RL typically use sparse reward signals, where a high positive reward is given only when the task is accomplished. To address this exploration

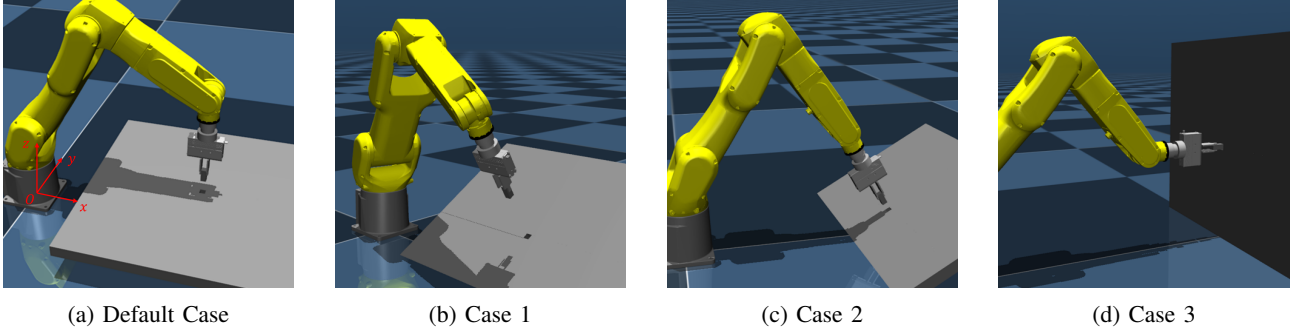


Fig. 1: Robot performing a peg into a hole insertion task in different scenarios for testing learning transferability. The data is collected, and the policy is trained only in performing the task shown in (a). The trained policy is then tested on the tasks shown in (b)-(d), where the insertion hole is translated in different orientations. (b): tilted in $+x$ direction for 30° (c): tilted in $-y$ direction for 30° (d): tilted in $-y$ direction for 90° . The coordinate frame is attached to the first figure.

issue, we leverage the off-policy nature of the SAC. Being off-policy, the trajectories in the replay buffer do not need to be sampled directly based on the current policy. As a result, we sample trajectories using the scripted expert policy every 10 epoch and inject them into the replay buffer to mitigate distributional shift issue.

Minimalist approach to solve PiH task via RL

We propose to use a minimalist approach to solving PiH tasks using RL by reducing the dimension of the action space to 2, denoted as $a_{RL} = [a_{RL1}, a_{RL2}]$. To map this reduced action space back to the original action space, we define $a = [a_{RL1}, a_{RL1}, a_{RL2}, 1, 1, 1]^T$. This proposal is motivated by several reasons. First, we observed a symmetric pattern in the expert policy design to finish the task. The rotational gains can always be set to their maximum value, and the gains in the x and y directions can be considered symmetric. By enforcing a symmetric structure and reducing the action space, the RL agent can learn the policy more efficiently as it does not need to explore unnecessary nonsymmetric action spaces. Additionally, compared to utilizing the full 6 degrees of freedom (DOF) gains, RL agents with smaller action spaces show more consistent learning dynamics.

The following reward function is considered for RL.

$$\begin{aligned}
 r(s, a) &= r_1 + r_2 + r_3 \\
 r_1 &= -0.1 \cdot \Psi(g, g_d) \\
 r_2 &= \begin{cases} 120 & \text{if } (z - z_d) < 0.026 \\ 0.04 - (z - z_d) & \text{else if } (z - z_d) < 0.04 \\ 0 & \text{otherwise} \end{cases} \quad (18) \\
 r_3 &= \begin{cases} -0.005 \cdot |f_{e_z}| & \text{if } d_p(p, p_d) > 0.002 \\ 0 & \text{otherwise} \end{cases}
 \end{aligned}$$

where $p = [x, y, z]^T$, $p_d = [x_d, y_d, z_d]^T$, f_{e_z} is a force sensor input in body frame z direction, and $d_p(p, p_d) = \sqrt{(x - x_d)^2 + (y - y_d)^2}$, with $\Psi(g, g_d)$ is a distance metric (10). Note that the weighting constants are selected heuristically and will vary in different applications and simulation setups.

V. EXPERIMENTS AND DISCUSSIONS

A. Behavior Cloning (BC)

The results of the BC experiments are presented in Table I. Each task was tested 100 times, and the success cases were counted. The BC policy trained with the GCEV and

TABLE I: Success rates of the BC and RL policies for the proposed and the benchmark approaches (Tested 100 times each, Values in Percentage %)

Method	Default	Case 1	Case 2	Case 3
BC Proposed (GIC+GCEV)	100	100	94	100
BC Benchmark (CIC+CEV)	100	0	8	17
BC Mixed 1 (GIC+CEV)	99	97	59	9
BC Mixed 2 (CIC+GCEV)	100	0	6	16
RL Proposed (GIC+GCEV)	100	96	100	100
RL Benchmark (CIC+CEV)	100	0	0	5

executed with the GIC (GIC+GCEV) successfully transferred the trained policy to the other tasks, without significant drop in the success rate. However, the BC policy trained with a CEV and executed with CIC (CIC+CEV) failed to transfer the trained policy, resulting in a dramatic decrease in the success rate. The reason for this difference in transferability can be attributed to the error vector representation. The relationship between left invariance and transferability is further explained in Remark 1.

Remark 1: Why does left-invariance matter?

The left-invariance of the error vector implies that the chosen error vector is invariant to the selection of the coordinate system. In this paper, we interpret left-invariance in a slightly different manner. Consider the situation where the desired and current configurations are transformed through a left action of the SE(3) group, which corresponds to a change in the spatial coordinate frame – See Fig. 2. Due to the left-invariance of the GCEV (11), the error vector remains unchanged in cases (a) and (b) in Fig. 2. Therefore, from the perspective of the proposed approach, the task remains invariant to translational/rotational perturbations. In this perspective, the use of the left-invariant error vector e_G can help address distributional shift or out-of-distribution issues, as the trained policy will consistently encounter the same input e_G .

B. Reinforcement Learning (RL)

The model with the highest validation return is chosen for evaluation. Experimental results in the 5th and 6th rows of Table I indicate that both the proposed and benchmark approaches achieved nearly perfect success rates in the training environment. However, the benchmark approach failed

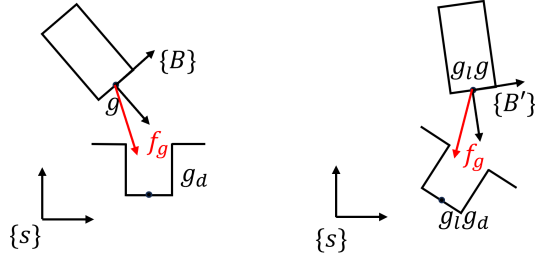


Fig. 2: (Left) Peg and hole configurations are represented by g and g_d , respectively. (Right) Peg and hole undergo transformation via an action $g_l \in SE(3)$. The GCEV e_G (11) and elastic force f_G (7) are invariant to the left transformation of $SE(3)$. $\{s\}$ represents spatial coordinate frame, while $\{B\}$ and $\{B'\}$ represent body coordinate frames.

to transfer the trained policy to different tasks, resulting in lower success rates as compared to the BC results. This could be attributed to the overfitting of the RL policy to the default case due to its reward maximization property.

C. Left-Invariance is not enough

The question arises whether training a policy based on GCEV or equivalent left-invariant features enables transferability to translational/rotational perturbations. To answer this question, we test different combinations of trained gain scheduling policies and control methods: BC policy with Cartesian error vector executed with GIC (GIC+CEV) and BC policy with GCEV executed with CIC (CIC+GCEV). If left-invariance of the feature were the only factor for transferability, we would expect the BC policy with the Cartesian error vector executed with GIC (GIC+CEV) to not be transferable due to the lack of left-invariance in the Cartesian error vector. Conversely, the BC policy with GCEV executed with CIC would be transferable.

However, the experimental results presented in 3rd and 4th rows of Table I contradict the hypothesis. GIC with a gain scheduling policy trained with the Cartesian error vector (GIC + CEV) showed some transferability in Case 1 and Case 2, with success rates higher than 50% and even reaching around 95%. However, in Case 3, with a tilt of 90 degrees, the trained policy failed due to encountering an unexperienced state distribution. This suggests that a left-invariant gain scheduling policy alone is not enough for transferability.

On the other hand, CIC with GCEV produced results consistent with our hypothesis. Even though the gain scheduling policy for CIC was trained with GCEV, the direction of the gains and resulting force direction are still represented in the Cartesian frame. Thus, the policy outputs the same gains it was trained on, but the resulting force direction is not suitable for tilted cases – see in Fig. 3.

Consequently, it is concluded that the left-invariant gain scheduling policy alone is not enough, and a more fundamental factor is needed to address transferability - the direction of forces. Unlike CIC, the forces in GIC are defined in the body frame, resulting in the automatic change in the direction

of forces (See Fig. 2, f_G on each case) – which implies an **equivariance** property. We state that the key to transferability lies in a control law represented in the body-frame coordinate and the left-invariant gain scheduling policy. The invariant gain scheduling policy is obtained from the neural network with GCEV as input, while the left-invariant feedback control law is inherited from the structure of GIC. To establish a connection between our statement and the equivariance property, we first present the definition of equivariance.

Definition 1: Consider a function $h : \mathcal{X} \rightarrow \mathcal{Y}$, i.e., $y = h(x)$ with $x \in \mathcal{X}$ and $y \in \mathcal{Y}$. The function h is equivariant to the group g if the following condition is satisfied [4]:

$$h(\rho^x x) = \rho^y h(x) \quad (19)$$

where ρ^x represents the action of group g in the domain \mathcal{X} and ρ^y represents the action of group g in the codomain \mathcal{Y} .

Based on Definition 1, we propose the following proposition.

Proposition 2: The feedback terms in GIC law (6) described in the body frame are equivariant if it is described in the spatial frame.

Proof: Consider the feedback terms $f_G(g, g_d)$ (7) and $e_V(g, g_d)$ (8), which are denoted on the body frame. See Fig. 2 for the coordinate systems. To show the equivariance property, we first show that the invariance on the body frame implies equivariance on the spatial frame.

Let $f_G^s(g, g_d)$ be $f_G(g, g_d)$ denoted in the spatial frame $\{s\}$. We note that g and g_d are described on the spatial frame $\{s\}$. Then, the left-transformed elastic force can be denoted by $f_G(g_l g, g_l g_d)$ on the transformed body frame $g_l g$ and is left-invariant by lemma 1, i.e., $f_G(g_l g, g_l g_d) = f_G(g, g_d)$. We now consider the left-transformed elastic force $f_G^s(g_l g, g_l g_d)$ with respect to the spatial frame $\{s\}$. The coordinates of the wrenches between the body and the spatial frame can be transformed by the following equations (see Ch. 2.5 of [6]):

$$f_G^s(g, g_d) = \text{Ad}_{g^{-1}}^T f_G(g, g_d) \quad (20)$$

$f_G^s(g_l g, g_l g_d) = \text{Ad}_{(g_l g)^{-1}}^T f_G(g_l g, g_l g_d) = \text{Ad}_{g_l^{-1} g^{-1}}^T f_G(g, g_d)$, where the Adjoint map is defined in (8). Therefore, the following equations hold:

$$\begin{aligned} f_G^s(g_l g, g_l g_d) &= \text{Ad}_{g_l^{-1} g^{-1}}^T (\text{Ad}_{g^{-1}}^T)^{-1} f_G^s(g, g_d) \\ &= (\text{Ad}_g \text{Ad}_{g_l^{-1}})^T f_G^s(g, g_d) = \text{Ad}_{g_l^{-1}}^T f_G^s(g, g_d), \end{aligned} \quad (21)$$

where we use a composition rule for the Adjoint map, $\text{Ad}_{g_1} \text{Ad}_{g_2} = \text{Ad}_{g_1 g_2}$, and an inverse property of the Adjoint map, $(\text{Ad}_g^T)^{-1} = \text{Ad}_{g^{-1}}^T$. Here, the domain \mathcal{X} in Def. 1 is $SE(3)$ (g or g_d), and the representation ρ^x is g_l , while the codomain \mathcal{Y} is $se^*(3)$ ($f_G^s(g, g_d)$ or $f_G^s(g_l g, g_l g_d)$) and the representation ρ^y is $\text{Ad}_{g_l^{-1}}^T$. Therefore, $f_G^s(g, g_d)$ is equivariant in $SE(3)$.

Similarly, to show the equivariance of $e_V(g, g_d)$ (8) on the spatial frame, the invariance on the body frame is only needed. The body frame velocities V^b and V_d^b are invariant to the left transformation since it is defined on the body frame and the Adjoint map $\text{Ad}_{g_b d}$ is invariant as the relative transformation matrix $g_b d = g^{-1} g_d$ is invariant to the left transformation. As a result, the feedback terms in GIC law

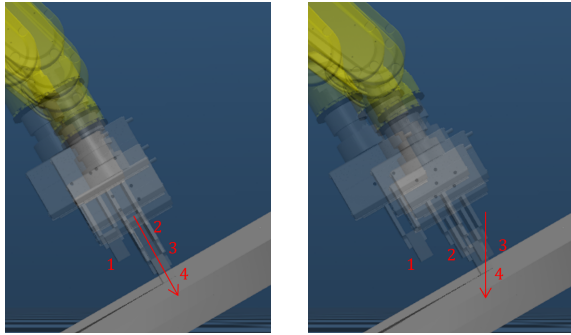


Fig. 3: Time-snap plots of for PiH task executed by (Left) GIC with GCEV, and (Right) CIC with GCEV. The numbers in the figure denote the time snap index, and the red arrow denotes the insertion direction. The desired point is located at the tip of the arrow. While GIC successfully first aligns with the axis of the hole as expert policy, CIC first aligns with the Cartesian z axis as it is trained in the default case (Fig. 1(a)).

(6) are equivariant in $SE(3)$. ■

Note that we only consider feedback terms in (6) since the feedforward terms are just employed to cancel the manipulator dynamics, not affecting the closed-loop dynamics. A few remarks on the Proposition 2 are provided.

Remark 2: Comments on Proposition 2

Lack of right-equivariance: The equivariance property suggested in Proposition 2 is equivalent to the left-equivariance or scene-equivariance in [28], which is weaker equivariance compared to the bi-equivariance proposed in [10]. The lack of right-equivariance was handled via sampling, as suggested in Proposition 1.

Extensions to force-based policy: It is worth mentioning that our concept can also be extended to general force-based policies. If a force-based policy is left-invariant in the body-frame, e.g., implemented using a neural network with left-invariant features as input, and described in the end-effector body frame, it will be guaranteed to be left-equivariant in the spatial frame. The GCEV (11) introduced in this paper is an example of such a left-invariant feature. We only consider deterministic policy in this paper, but a probabilistic policy can also be considered. In such cases, the equivariant probabilistic policy implies invariance of the conditional probabilities when the state and action are equivariantly transformed [28].

VI. HARDWARE EXPERIMENT

To validate the proposed concept, we implemented our methods on the hardware robot; Fanuc 200iD/7L. For the hardware implementation and ease of implementation, we modify the GIC (geometric impedance control) to the Geometric Admittance Control (GAC) law. To define the admittance control version of the GIC (GAC), the desired closed-loop control system $M\dot{e}_V + K_d e_V + f_G(g, g_d) = \tilde{T}_e$ is first considered, where M is a fixed desired inertia matrix, K_d is a fixed damping matrix, \tilde{T}_e is an external force acting on the end-effector, and f_G is our beloved elastic wrench (7) in $SE(3)$. Since our task is PiH, we again fixed the desired configuration g_d as a constant, which leads to the following

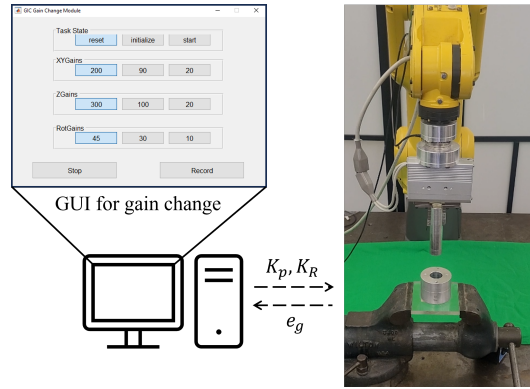


Fig. 4: Schematic for the data collection method is shown. A robot executes the geometric admittance control for the PiH task, and an expert watching the process changes the gains via a GUI in real-time.

desired closed-loop system:

$$M\dot{V}^b + K_d V^b + f_G(g, g_d) = \tilde{T}_e. \quad (22)$$

In what follows, we formulate (22) into a discrete-time setting for the derivation of the admittance control law.

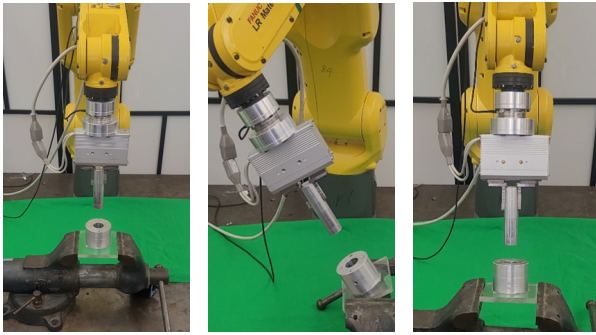
$$V^b(k+1) = V^b(k) + \Delta t \cdot M^{-1} \left(f_G(k) + K_d V^b(k) + \tilde{T}_e(k) \right),$$

where we use $f_G(k)$ to denote $f_G(g, g_d)$ at k instance for simplicity, and Δt is a sampling time. The $V^b(k+1)$ term can then be considered to be the desired velocity at the $k+1$ instance. Thus, the geometric admittance control law now boils down to a joint-space velocity PD control, with desired joint-space velocity $\dot{q}_d(k)$ given as $\dot{q}_d(k) = (J_b(k))^{-1} V^b(k)$. For the impedance learning problem, the dataset $\{(e_G, (K_p, K_R))\}_{i=1}^N$ is required. The data collection process is summarized in Fig. 4. The robot is provided with $g_d = (R_d, p_d)$ and is controlled by the GAC to execute a PiH task. The human expert supervising this task process changes the gains (K_p, K_R) of GAC in real-time using the GUI, and the gain signals are sent to the manipulator with an ethernet UDP communication protocol. The output signal e_G is received from the communication module and is recorded alongside the gain command signal as the dataset. We collected 75 trajectories, which sums up to $\sim 250k$ of dataset size. Similar to the simulation experiment, we also collected data and trained policy only on the default case, and tested on the tilted cases, as summarized in Fig. 5. We set the failure case when the peg is stuck to the whole, e.g., the task cannot be completed within 60s.

The result of the hardware validation is presented in Table II. As can be seen in the result, the proposed approach of utilizing GIC (or GAC) together with the gain scheduling policy implemented with GCEV showed perfect success rates, and the trained policy was transferrable to previously unseen cases.

VII. CONCLUSIONS

In this paper, a geometric approach leveraging $SE(3)$ group invariance and equivariance for contact-rich robotic manipulation task learning is presented. To solve the Peg-in-Hole (PiH) task, the proposed approach builds on top of



(a) Default case (b) Case 1 (c) Case 2

Fig. 5: (a) Default case where the data is collected, and the BC policy is trained. The trained policy is then directly tested on the holes with different positions/orientations. The hole is tilted (b) 30° in $+x$ axis, (c) -22.5° in $+y$ axis.

TABLE II: Success rates of the BC policy for the proposed approach in the hardware implementation (Tested 10 times each, Values in Percentage %)

Method	Default	Case 1	Case 2
Proposed (GAC+GCEV)	100	100	100

the geometric impedance control (GIC), where its impedance gains are changed via a left-invariant gain scheduling policy. Expert behavior cloning and deep reinforcement learning are chosen for training the gain scheduling policy. Through theoretical analysis, we prove that the proposed GIC and the geometrically consistent error vector (GCEV) used for learning are left-invariant relative to $SE(3)$ group transformations when represented in the end-effector's body frame system, enabling learning transferability. Furthermore, we show that left invariance in the body-frame representation leads to $SE(3)$ equivariance of the proposed approach when described in a spatial frame. A PiH simulation experiment confirms the learning transferability of our proposed method, which is not exhibited by the well-known Cartesian-space based benchmark approach. These results are further validated on an actual PiH robotic hardware implementation, and the pipeline for the hardware implementation is also presented.

REFERENCES

- [1] H. Ravichandar *et al.*, "Recent advances in robot learning from demonstration," *Annual review of control, robotics, and autonomous systems*, vol. 3, pp. 297–330, 2020.
- [2] X. Zhang *et al.*, "Learning variable impedance control via inverse reinforcement learning for force-related tasks," *IEEE Robotics and Automation Letters*, vol. 6, no. 2, pp. 2225–2232, 2021.
- [3] C. C. Beltran-Hernandez *et al.*, "Variable compliance control for robotic peg-in-hole assembly: A deep-reinforcement-learning approach," *Applied Sciences*, vol. 10, no. 19, p. 6923, 2020.
- [4] T. Cohen and M. Welling, "Group equivariant convolutional networks," in *International conference on machine learning*. PMLR, 2016, pp. 2990–2999.
- [5] E. J. Bekkers *et al.*, "Roto-translation covariant convolutional networks for medical image analysis," in *Medical Image Computing and Computer Assisted Intervention—MICCAI 2018: 21st International Conference, Granada, Spain, September 16-20, 2018, Proceedings, Part I*. Springer, 2018, pp. 440–448.

- [6] R. M. Murray, Z. Li, and S. S. Sastry, *A mathematical introduction to robotic manipulation*. CRC press, 1994.
- [7] J. Seo *et al.*, "Geometric impedance control on $SE(3)$ for robotic manipulators," *IFAC World Congress 2023, Yokohama, Japan*, 2023.
- [8] A. Zeng *et al.*, "Transporter networks: Rearranging the visual world for robotic manipulation," in *Conference on Robot Learning*. PMLR, 2021, pp. 726–747.
- [9] A. Simeonov *et al.*, "Neural descriptor fields: $SE(3)$ -equivariant object representations for manipulation," in *2022 International Conference on Robotics and Automation (ICRA)*. IEEE, 2022, pp. 6394–6400.
- [10] H. Ryu *et al.*, "Equivariant descriptor fields: $SE(3)$ -equivariant energy-based models for end-to-end visual robotic manipulation learning," in *The Eleventh International Conference on Learning Representations (ICLR)*, 2023.
- [11] N. Thomas *et al.*, "Tensor field networks: Rotation-and translation-equivariant neural networks for 3d point clouds," *arXiv preprint arXiv:1802.08219*, 2018.
- [12] T. Inoue *et al.*, "Deep reinforcement learning for high precision assembly tasks," in *2017 IEEE/RSJ International Conference on Intelligent Robots and Systems (IROS)*. IEEE, 2017, pp. 819–825.
- [13] S. Kozlovsky, E. Newman, and M. Zacksenhouse, "Reinforcement learning of impedance policies for peg-in-hole tasks: Role of asymmetric matrices," *IEEE Robotics and Automation Letters*, vol. 7, no. 4, pp. 10 898–10905, 2022.
- [14] K. M. Lynch and F. C. Park, *Modern robotics*. Cambridge University Press, 2017.
- [15] O. Khatib, "A unified approach for motion and force control of robot manipulators: The operational space formulation," *IEEE Journal on Robotics and Automation*, vol. 3, no. 1, pp. 43–53, 1987.
- [16] F. Bullo and R. M. Murray, "Tracking for fully actuated mechanical systems: a geometric framework," *Automatica*, vol. 35, no. 1, pp. 17–34, 1999.
- [17] T. Lee *et al.*, "Geometric tracking control of a quadrotor uav on $SE(3)$," in *49th IEEE conference on decision and control (CDC)*. IEEE, 2010, pp. 5420–5425.
- [18] F. Caccavale *et al.*, "Six-dof impedance control based on angle/axis representations," *IEEE Transactions on Robotics and Automation*, vol. 15, no. 2, pp. 289–300, 1999.
- [19] Y. Zhu *et al.*, "robosuite: A modular simulation framework and benchmark for robot learning," in *arXiv preprint arXiv:2009.12293*, 2020.
- [20] H. Ochoa and R. Cortesão, "Impedance control architecture for robotic-assisted mold polishing based on human demonstration," *IEEE Transactions on Industrial Electronics*, vol. 69, no. 4, pp. 3822–3830, 2021.
- [21] S. Shaw, B. Abbatematteo, and G. Konidaris, "RMPs for safe impedance control in contact-rich manipulation," in *2022 International Conference on Robotics and Automation (ICRA)*. IEEE, 2022, pp. 2707–2713.
- [22] E. Todorov, T. Erez, and Y. Tassa, "Mujoco: A physics engine for model-based control," in *2012 IEEE/RSJ International Conference on Intelligent Robots and Systems*. IEEE, 2012, pp. 5026–5033.
- [23] "Berkeley RL Kit," <https://github.com/rail-berkeley/rllkit>, accessed: 2023-07-01.
- [24] J. Tobin *et al.*, "Domain randomization for transferring deep neural networks from simulation to the real world," in *2017 IEEE/RSJ international conference on intelligent robots and systems (IROS)*. IEEE, 2017, pp. 23–30.
- [25] T. Haarnoja *et al.*, "Soft actor-critic: Off-policy maximum entropy deep reinforcement learning with a stochastic actor," in *International conference on machine learning*. PMLR, 2018, pp. 1861–1870.
- [26] H. Yong *et al.*, "Suspension control strategies using switched soft actor-critic models for real roads," *IEEE Transactions on Industrial Electronics*, vol. 70, no. 1, pp. 824–832, 2022.
- [27] A. Y. Yasutomi, H. Mori, and T. Ogata, "A peg-in-hole task strategy for holes in concrete," in *2021 IEEE International Conference on Robotics and Automation (ICRA)*. IEEE, 2021, pp. 2205–2211.
- [28] J. Kim *et al.*, "Robotic manipulation learning with equivariant descriptor fields: Generative modeling, bi-equivariance, steerability, and locality," in *RSS 2023 Workshop on Symmetries in Robot Learning*, 2023.